MODELLING AND SIMULATION OF ELECTROMAGNETIC EFFECTS IN SPACE MECHANISMS

F. Liebold [(1)], C. Allegranza [(1)], R. Seiler [(1)], A. Junge [(2)]

[(1)] *ESA/ESTEC – Mechanisms Section, P.O. Box 299, 2200 AG Noordwijk, The Netherlands*
Email: florian.liebold@esa.int, claudia.allegranza@esa.int, rene.seiler@esa.int
[(2)] *ESA/ESTEC – Electromagnetic Compatibility Section, P.O. Box 299, 2200 AG Noordwijk, The Netherlands*
Email: axel.junge@esa.int

ABSTRACT

When developing electromagnetic devices, modelling and simulation techniques have become powerful tools to facilitate and accelerate the engineering process. This is particularly relevant for space applications in science and Earth observation where the requirements on mechanisms equipment tend to be very mission specific, so that commercial off-the-shelf items cannot be used. With custom designs, the effort on hardware breadboarding and development models might be limited. Therefore there is a high potential to reduce overall development effort and associated cost by an early start of a model assisted approach.

The paper discusses the model generation process in a Finite Element Analysis (FEA) environment, including the representation of mechanism components e.g. electric motors and bearings, as well as the external environment in order to cover far-field effects. Particular attention is given to magnetic shielding as currently investigated for future ESA missions, for instance, Solar Orbiter. An approach to correlate the analysis results with test data is outlined, and the necessary test facilities are briefly described. Further electromagnetic effects relevant for space mechanisms comprise eddy current induced losses and magnetic hysteresis where future investigations are planned in order to minimise undesired effects or to optimize performance.

INTRODUCTION

Many actuators and sensors that are used in space mechanisms rely on electromagnetic principles for their function and operation. Therefore, the optimisation of related design features and the resulting performance has become a relevant and promising area for investigation. State-of-the-art software tools allow for a detailed analysis of design options, using two- or three-dimensional finite element models already very early in the overall development process. This is a particularly powerful approach for highly customised design solutions and feasibility studies for new concepts when design heritage and hardware prototype test data are not available yet.

In addition to DC characteristics, recently AC magnetic cleanliness of spacecraft equipment has become a critical requirement as well, in particular for upcoming ESA science missions such as BepiColombo, Solar Orbiter and JUICE. Especially, time-varying magnetic fields constrain the capabilities of sensitive scientific instruments, for instance high-performance magnetometers. During the design of space mechanisms, a number of measures can be taken to reduce the remanent magnetic dipole moment, in order to meet the stringent requirements of new science missions.

In order to support any future development in the direction of 'magnetically clean' mechanisms, the capabilities of electromagnetic simulation software such as ANSYS® Maxwell have been assessed. In this frame, the need for a close interaction between the modelling & simulation process and hardware measurements is emphasised.

MODELLING AND SIMULATION

Software Tools

The software tool used in the frame of this study is ANSYS® Maxwell Version 16 [1], a FEM based electromagnetic modelling and simulation tool. It is used to compute the generation and propagation of electromagnetic fields in a 3 D environment and to determine the interaction of electromagnetic fields with hardware items in terms of resulting forces, e.g. reluctance or Lorentz forces, and induced eddy currents. The software is capable of performing magneto-static as well as time-variant transient analyses. Both were performed in the frame of this study. The software uses an adaptive meshing algorithm, which facilitates the control of the accuracy of the analysis results as well as the computation time.

Magnetic Source Modelling

In the frame of this study, it has been attempted to reproduce the magnetic characteristics of a typical actuator operating at high speeds, i.e. 4000 rpm, with
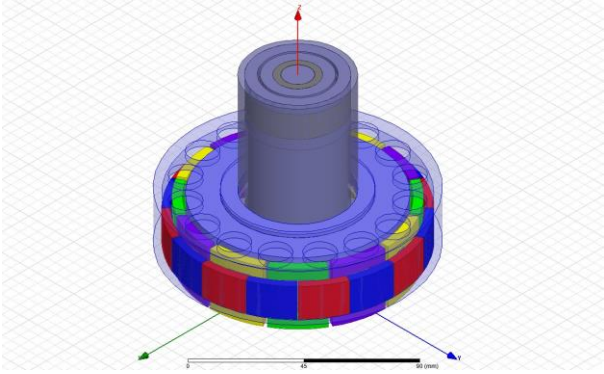
Figure 1: Geometric depiction of DC motor drive unit

relatively high motor power. For this purpose a direct-drive DC electric motor with 16 permanent magnets and a set of AISI 440 C stainless steel ball bearings has been modelled according to *Figure 1*. It is assumed that this kind of configuration possesses adverse properties in terms of generation of DC and AC magnetic fields. This is due to the large number of permanent magnets sitting on the rotor part of the motor unit on a circumference with radius 150 mm. The air gap between permanent magnets and back iron has been set to 10 mm to allow for the generation of magnetic stray fields.

Since ferritic and martensitic steels such as AISI 440 C are known to become magnetized through exposure to ambient magnetic fields as well as mechanical loads, e.g. during manufacturing or mechanical testing, the outer rings of the ball bearings have been modelled as magnetic dipoles by appropriate selection of the respective material properties, cf. *Table 1*.

Table 1: Relevant material properties to model the magnetic characteristics of the actuator

Part	Relative Permeability $\mu_{r,nom}$ [-]	Coercive Field Strength B_c [A/m]	Bulk Conductivity [S/m]
Magnet Carrier	800	0	1666666.67
Back Iron	800	0	1250000.00
Inner Spacer	800	0	1250000.00
Outer Spacer	800	0	1250000.00
Ball bearing balls	800	0	1250000.00
Ball bearing outer race	800	40*	1250000.00
Ball bearing inner race	800	0	1250000.00
Shaft	200	0	2044989.78
Spring	200	0	2044989.78
Magnets	1.094190234	800,000*	1111111.11

Parts made from non-ferromagnetic materials such as aluminium are not depicted in the figure and are only relevant when it comes to the computation of eddy current induced loss torques. Aluminium as a paramagnetic material does hardly interfere with magnetic fields, i.e. the relative magnetic permeability μ_r is close to 1 [2], and is not prone to becoming inadvertently magnetised.

During the course of this study, the influence of certain modelling parameters on the overall magnetic characteristics has been analysed. This regards in particular the coercive field of the motor magnets as well as the bearing steel which is subject to a certain variability due to manufacturing tolerances or systematic demagnetization.

Meshing and Sizing

Due the adaptive meshing algorithm implemented in the software, the mesh size increases significantly in free space. The default meshing process puts emphasis on areas with high geometric complexity as shown in *Figure 2*. Since it is the far-field characteristics that are of interest in this study, the mesh has been refined by placing "sheets" in the free space that do not have any physical properties, but cause the creation of mesh nodes across their surfaces.
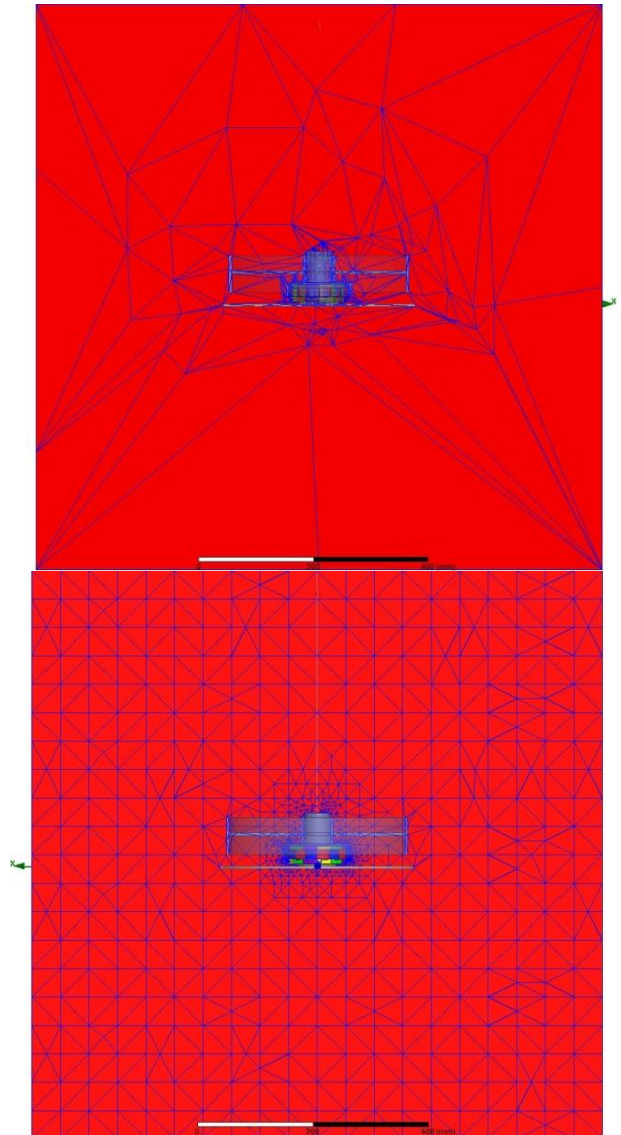
Figure 2: Coarse and fine mesh in the external simulation space

The maximum magnitude of the magnetic flux density B caused by a perfect magnetic dipole with magnetic moment magnitude m decays with $1/r^3$ with r being the distance from the dipole:

$$B = \frac{\mu_0}{2\pi} \cdot \frac{m}{r^3}$$ **Eq. 1**

Since the actuator model represents a rather complex geometry with multiple magnetic sources, this assumption is not true in the close vicinity of the actuator hardware due to local effects such as cancellation, shielding, guidance and leakage of the magnetic field. Hence, it was investigated at which distance the simulated magnetic flux density meets aforementioned assumptions in all three dimensions.

According to *Figure 3*, this is the case in a range of about 200 mm to 400 mm radial distance from the centre of the motor. At distances further than that, boundary effects due to the limitation of the simulation volume appear. Therefore a radial distance of about 300 mm was chosen to determine a magnetic dipole moment representative for the actuator as a whole. Magnetic dipole moments given in this document have been calculated at that range.
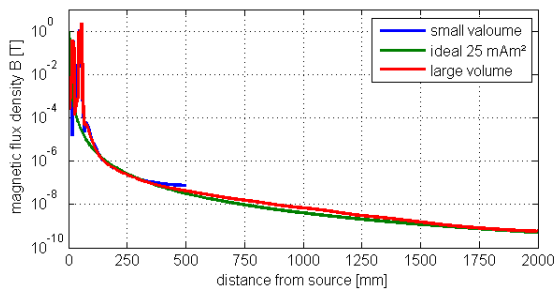
Figure 3: Magnetic flux density caused by the actuator model at different radial distances from the motor centre (the orange curve showing the ideal flux density calculated using Eq.1)

As can be seen in *Figure 3*, the far-field assumption is true in a larger range using a larger simulation volume, e.g. beyond 2 m as in the shown case. However, in order to limit the calculation time to below 1 hour per run, the simulation volume was chosen to be 1 x 1 x 1 m^3.

DC Field Emissions

Different measures can be taken in order to reduce the remaining magnetic dipole moment of mechanisms. In the frame of this study, the effectiveness of different magnetic shielding configurations has been investigated by magneto-static analysis. Furthermore, the impact of reduced magnet variability as well as the effect of demagnetized ball bearing rings has been analysed.

a)   Assessment of Shielding Effectiveness

In the frame of this study, a variety of shielding configurations was modelled and assessed. As shielding material Mu-metal has been selected, for the modelling of which the default parameters by ANSYS Maxwell have been used. These feature a non-linear B-H-curve with a variable relative permeability depending on the magnitude of the magnetic field H, which is given in *Figure 4*. As can be seen, the given B-H curve increases almost linear at low field strengths, representing a magnetic permeability μ_r of about 80,000 according to Eq. 2. This is a rather high value provided that most manufacturers of mu-metal specify a permeability of about 50,000 [3]. Simulation results of the presented case suggest that the material behaves linear since the observed magnetic field strengths does not exceed H = 0.1 A/m at the location of the shields.

$$B = \mu_0 \cdot \mu_r \cdot H$$ **Eq. 2**
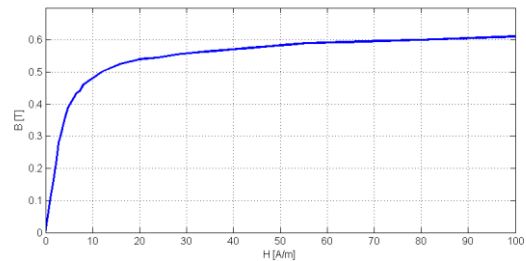
Figure 4: Default B-H curve of Mu-metal in ANSYS® Maxwell
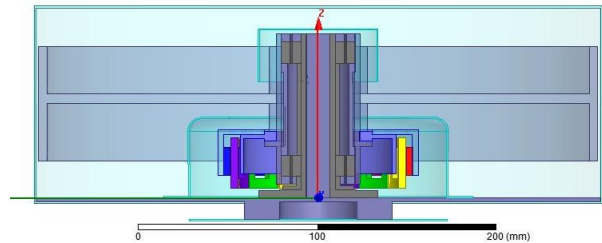
Figure 5: Depiction of different shielding elements implemented in the actuator design (including internal and external shielding options)

In a first simulation campaign, the influence of certain geometric parameters of the shielding design, shielding thickness and shielding radius, has been assessed by performing parametric sweeps. *Figure 6* shows, per example, the influence of the lower shielding radius (encapsulating the motor as shown in *Figure 5*) on the magnetic flux generated by the actuator. Unlike intuitively guessed, the flux density reduces with increasing distance of the shield from the source. The effect however is minor. It is assumed that the reason for this deviation from theory is the absence of an enclosed shielding structure, hence enabling "leakage"
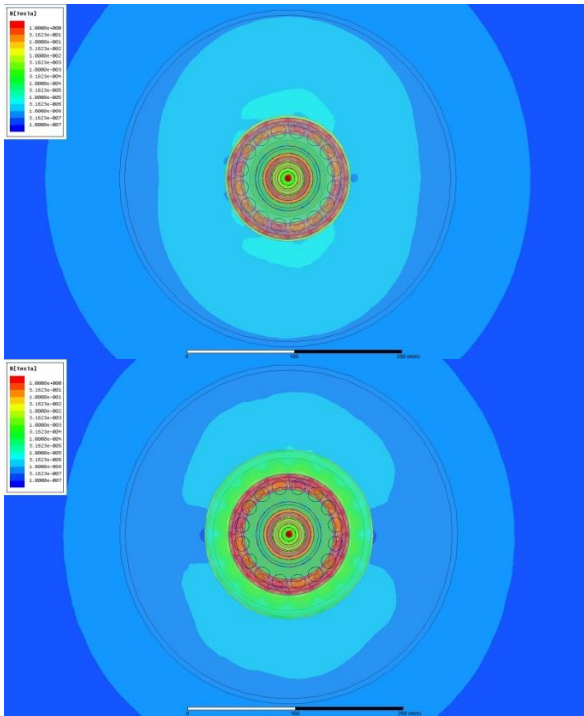
Figure 6: Magnetic flux density in horizontal plane at different shielding distances r from the rotor

of the magnetic field. In this case, also the increase of total shielding material volume becomes dominant.

Not very surprisingly, the shielding effectiveness increases with increasing shielding thicknesses. However, this effect is bounded as depicted in *Figure 7* where some asymptotic levelling of magnetic field reduction can be observed. According to this, shielding thicknesses greater than 1.5 mm do not have significant additional shielding effect.
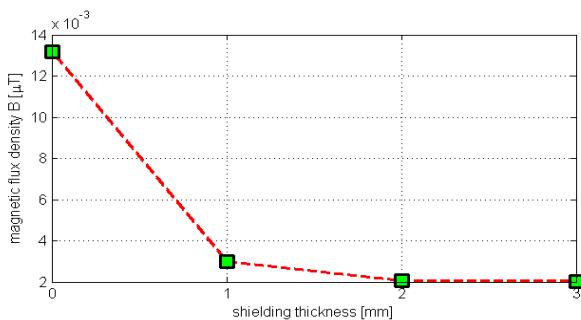
Figure 7: Magnetic flux density for different shield thicknesses

As shown in *Figure 5*, a variety of different shielding elements has been included in the actuator model. The effects of the different shielding elements on the remaining magnetic dipole moment have been assessed taking into account the individual shielding elements as well as combined shielding configurations.
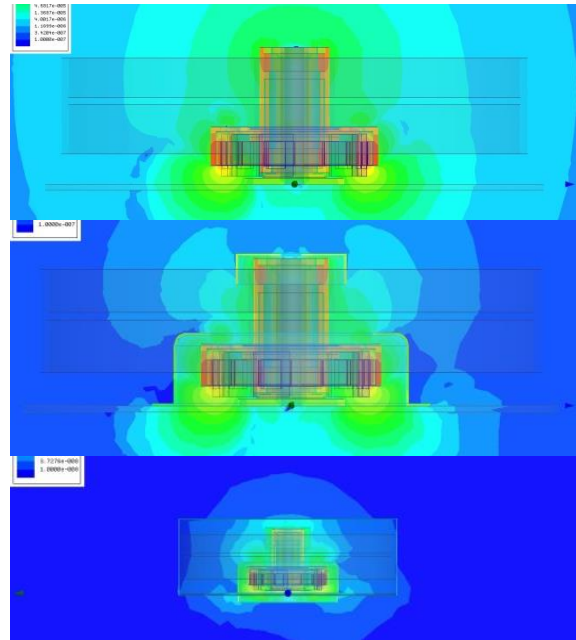
Figure 8: Visualization of magnetic flux density B at different shielding configurations ((1) unshielded, (2) upper and lower internal shielding, (3) combined internal and external shielding)

In the presented example the remaining magnetic dipole moment of the unshielded actuator of about 8.5 mAm² could be reduced by approx. 10 dB through the implementation of internal shielding elements as shown. Since those internal elements are no complete enclosures, stray fields in the lower part of the actuator limit the shielding effectiveness. An additional attenuation of the magnetic flux emission of approx. 25 dB is shown by means of an external Mu-metal shield with a thickness of 1 mm which is completely encasing the actuator.
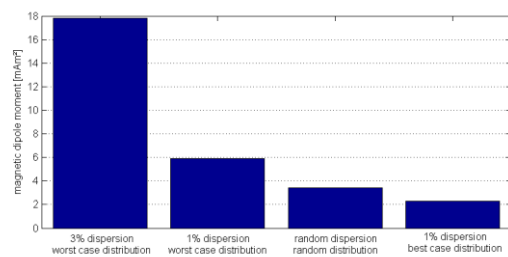
Figure 9: Magnetic dipole moments resulting from differently magnetized permanent magnets

b) Effect of Magnet Variability

The permanent magnets used in electric motors are subject to certain manufacturing tolerances, which are also affecting the magnetic properties of the parts. Typically, the remanence (i.e. remanent flux density) of one type of permanent magnets may vary within ± 3 %

of the specified value [4]. An asymmetric distribution of differently magnetized permanent magnets within the rotor assembly will result in an increased remaining dipole moment of the actuator. This has been quantified in the study assuming a 'worst-case', 'best-case' and random distribution of the differently magnetized magnets. Furthermore, the effects of a decreased magnet variability of ± 1 % has been assessed.

As shown in *Figure 9*, a significant improvement of the magnetic field emissions of the rotor unit can be achieved by reducing the dispersion of the remanence of the individual magnets. A further reduction is shown by an improved distribution of the magnets, i.e. equally magnetized magnets sitting on opposite sides of the rotor to achieve a symmetric distribution.

c) Parts Degaussing

As mentioned above, ferritic steels such as 440C are prone to becoming inadvertently magnetized through the application of mechanical stress or strong ambient magnetic fields. Magnetic field measurements on individual ball bearings have shown that this can result in remaining dipole moments of 20 to 100 mAm² of the finished parts which contributes significantly to the magnetic footprint of a mechanism. In the presented case a magnetic dipole moment of a ball bearing of about 20 mAm² has been modelled by assigning a coercive field strength of 40 A/m to the material of the outer races. The magnetic field vector was applied in radial direction, i.e. orthogonal to the spin axis of the rotor to allow a worst case contribution to the magnetic dipole moment of the mechanism.

Reduction of the inherent coercive field strength of ball bearings and other mechanical parts can be achieved by demagnetization methods, also known as de-perming or degaussing which is a process during which the affected parts are exposed to a strong AC magnetic field decaying over a period of 400 s [5]. It has been shown that thereby the magnetic dipole moment of ball bearings can be significantly reduced. The model representation of a magnetized ball bearing has been adjusted accordingly via adaptation of the coercive field.

DC AND AC MAGNETIC EMISSION MEASUREMENT APPROACH

In order to compare the above simulation results with actual test data a measurement campaign as shown below is planned using ESTEC's Mobile Coil Facility (MCF). The outlined test setup will be used to determine the DC and AC shielding effectiveness of metallic glasses based on Nickel and Cobalt.
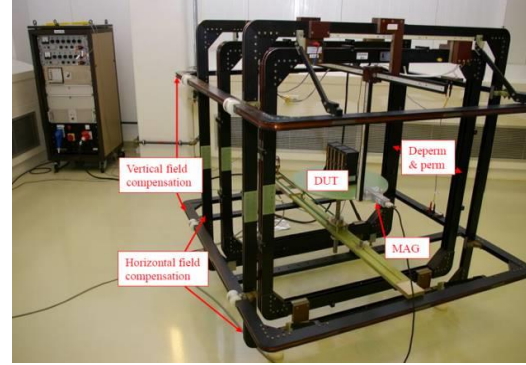
Figure 10: ESTEC Mobile Coil Facility "Ulysses"

As depicted in *Figure 10* the MCF consists of three pairs of Helmholtz coils, two of which are used to compensate the Earth's magnetic field: the facility's main axis is pointing to North, whereby no compensation is needed perpendicular to it, i.e. in East – West direction. The third pair of Helmholtz coils is used to perform de-perming according to ECSS-E-ST-20-07C Rev. 1 [5].

The facility includes a set of four magnetic field sensors type Mag-03MSL100 which can be placed in variable distances from the test object. This allows the sensors to be located in an optimal range in terms of sufficient signal-to-noise ratio and immunity against local stray fields.

A turntable in the centre of the setup allows for a 360° rotation of the device under test (DUT). Magnetic flux density B is measured during a full rotation and used to calculate the equivalent DC magnetic dipole moment of the DUT using different a fitting algorithms, e.g. Particle Swarm Optimization [8]. Furthermore, time domain data of the magnetic flux density can be sampled with several kHz sampling rate.

It is planned to perform DC and AC magnetic flux measurements on unshielded as well as a shielded DUTs, e.g. *Figure 11*. The shielding materials are typically available in form of ribbons with a width of about 50 mm and a thickness of just some 10 µm. They will be applied on the mechanism housing or on enclosures of representative shape and size. Using different kinds of magnetic sources, e.g. different permanent magnets between about 2 mAm² and 400 mAm² and a battery-driven DC electric motor with permanent magnet attached to the shaft, cf. [8], will allow to estimate the shielding effectiveness SE of a material in dependence of frequency and amplitude of the induced magnetic field. Moreover, the effect of multiple layers of shielding material can be investigated.

$$SE = 20 \cdot \log_{10} \frac{B_{\text{shielded}}}{B_{\text{unshielded}}} \qquad \textbf{Eq. 3}$$
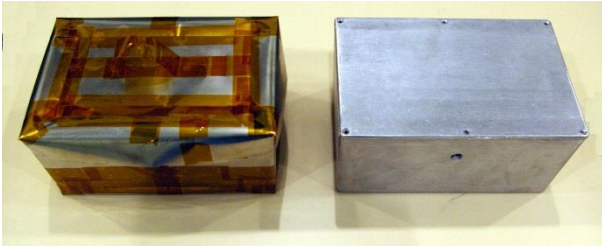
Figure 11: Example of shielding material applied to non-representative rectangular aluminium enclosure.
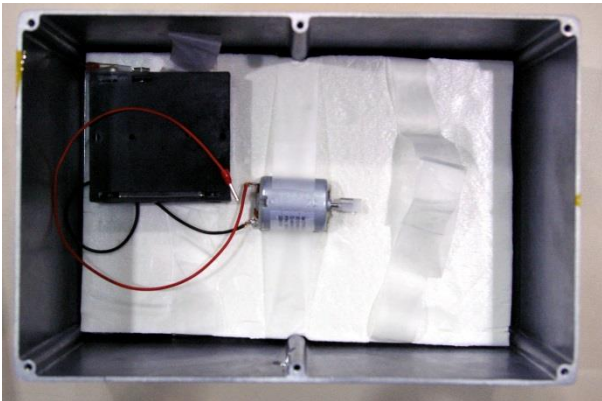
Figure 12: Electric motor with permanent magnet in non-representative Aluminium enclosure for generation of AC magnetic fields.

MODELLING OF EDDY CURRENT EFFECTS AND MAGNETIC HYSTERESIS

In the context of performance prediction and optimisation, the need for modelling of non-linear effects of electromagnetic devices becomes of primary importance. Typically, most relevant effects are eddy current losses and magnetic hysteresis effects, both of them leading to degradation of performances where unwanted. In some other cases they are in fact used on purpose for a certain functionality. As an example, eddy current dampers or brakes are quite broadly used in space applications and preferred due to their contactless design.

Modelling of eddy current effects may be quite complicated. Most software tools nowadays offer an automatic computing feature which considers conductivity of the bulk material and derives the related Joule losses while imposing a constant speed to the system. However, transient simulation accounting for non-linear mechanical and magnetic effects are very rare due to the computational effort and model complexity.

Up to now, magnetic hysteresis of materials is rarely modelled in existing commercial software tools for electromagnetic problems. A linear characteristic is typically considered for permanent magnets, and semi-

hard magnetic materials are typically considered as soft magnetic. In recent years, a lot of effort has been put into this topic by software developers. This development shall allow for simulations considering the magnetic hysteresis loop of relevant materials, minor loops included.

Study Case: Magnetic Hysteresis

A first attempt to use some new simulation features was recently made at ESA/ESTEC with the intention of studying a torque coupler based on hysteresis effects in more detail. The example device was developed to transfer the actuation torque to the outside of a sealed housing containing the motor. The same concept has been proposed as a brake device.

The device is composed of an inner part, the rotor with permanent magnets and an outer part, the stator which is made of laminations from a semi-hard magnetic material. The latter exhibits a large hysteresis loop similar to magnets, however, its demagnetizing field is lower. Therefore, it can be easily demagnetized by a field produced by classic permanent magnets.
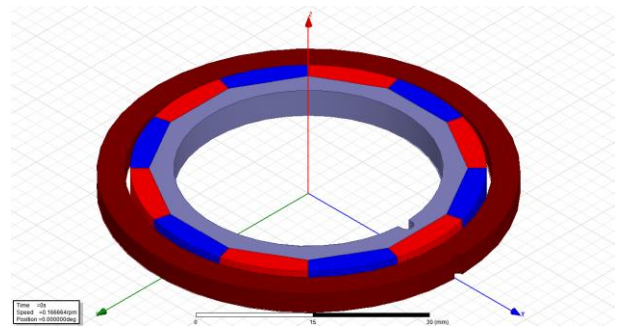
Figure 13: ANSYS Maxwell model of magnetic coupler

The working principle of the torque coupler is to behave like a mechanical coupler up to a certain level of torque with synchronous rotation of rotor and stator; once a predefined torque threshold is passed, the rotor starts sliding with respect to the stator on the output shaft, allowing for relative motion between input and output shaft, but without contact between the parts.

During preliminary functional test, a low mechanical rotational stiffness was observed during transient torque conditions, with a displacement vs. torque characteristic showing quite a large rotation (few degrees) before reaching the threshold torque value. The resulting curve presenting the torque and the angular position versus time is shown in *Figure 16*.

In a first step of simulation, the rotation speed of the rotor was imposed as constant. It was very easily possible to obtain the correct value of the coupling
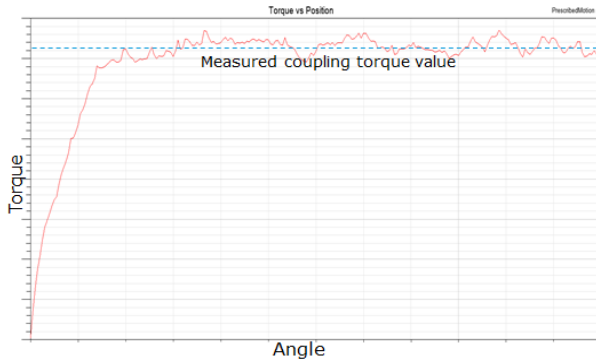
Figure 14: Torque vs. position characteristic with imposed motion of the rotor
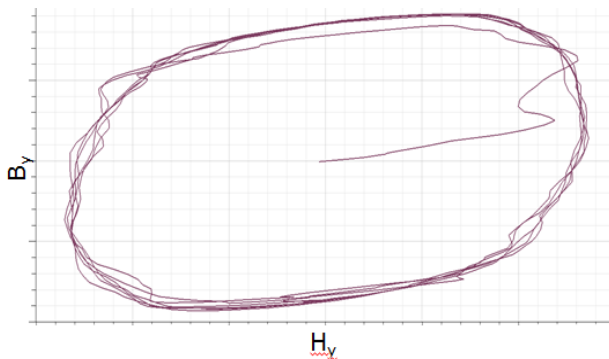
Figure 15: Hysteresis loops observed on the stator (single point) during simulation

torque. It was also possible to show the "spring effect". The simulation shows that the constant braking torque is reached only after a substantial relative rotation. This is certainly more than the measured value, but it has to be noted that the simulation starts with a completely non-magnetised stator. Thus, the magnetisation process has also to be taken into account.

In a second simulation step, a torque profile over time was imposed to the rotor, and the position was recorded. The torque profile was first linearly increased up to a value higher than the coupling torque and then kept at this level for a certain duration before dropping down to 0 Nm.
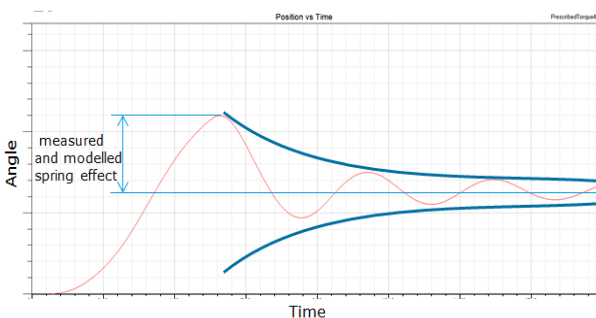
Figure 16: Rotor position vs. time during transient simulation

The resulting position shows that the rotor, as expected, starts to rotate up until the torque is kept at the high value. As soon as the torque is removed and due to absence of friction and low damping in the system, the rotor starts oscillating around a final equilibrium position. In this way, it was possible to reproduce exactly the back drive measured on the hardware. A close look at the magnetisation of the stator and the magnetic field of the rotor reveals that they are not aligned when the torque is transmitted. The phase shift corresponds quite precisely to the shown back drive.

CONCLUSIONS

Modelling and simulation of electromagnetic devices is becoming more and more commonly considered as a viable means for design and optimisation of performance. In this paper, most recent applications have been presented where a good correlation with measurement has been achieved. A deeper understanding of electromagnetic effects has been enabled, and the power of modern analysis tools for electromagnetic systems has been demonstrated.

REFERENCES

[1] http://www.ansys.com/Products/Simulation+Technology/Electronics/Electromechanical/ANSYS+Maxwell

[2] Albach, M. (2011). *Elektrotechnik*, Pearson, Munich, GER.

[3] Schnabel A., *Magnetic Shielding, National Metrology Institute of Germany*, Braunschweig, GER.

[4] Datasheet Recoma 28, Arnold Magnetic Technologies Corp.

[5] ECSS-E-ST-20-07C Rev1, *Electromagnetic compatibility*, 7 February 2012

[6] Anderson J.B., Hillenbrand M., Meyer P., *Magnetics Characterization of Flight ReactionWheels for MESSENGER*, 2003

[7] Allegranza C*., Actuators for Space Applications: State of the Art and New Technologies*, Actuator 2014, Bremen, 2014

[8] Carrubba, E., Junge, A., Marliani, F., and Monorchio, A., *Particle Swarm Optimization for Multiple Dipole Modeling of Space Equipment*, Trans. on Magn., vol. 50, no. 12, 2014, article 7028010